

# Divalent ion competition reveals reorganization of an RNA ion atmosphere upon folding

Robert J. Trachman, III<sup>1</sup> and David E. Draper<sup>2,\*</sup>

<sup>1</sup>Department of Biophysics, Johns Hopkins University, Baltimore, MD 21218, USA and <sup>2</sup>Department of Chemistry, Johns Hopkins University, Baltimore, MD 21218, USA

Received September 22, 2016; Revised December 14, 2016; Editorial Decision December 16, 2016; Accepted December 26, 2016

## ABSTRACT

Although RNA interactions with  $K^+$  and  $Mg^{2+}$  have been studied extensively, much less is known about the third most abundant cation in bacterial cells, putrescine<sup>2+</sup>, and how RNA folding might be influenced by the three ions in combination. In a new approach, we have observed the competition between  $Mg^{2+}$  and putrescine<sup>2+</sup> (in a background of  $K^+$ ) with native, partially unfolded and highly extended conformations of an adenine riboswitch aptamer. With the native state, putrescine<sup>2+</sup> is a weak competitor when the ratio of the excess  $Mg^{2+}$  (which neutralizes phosphate charge) to RNA is very low, but becomes much more effective at replacing  $Mg^{2+}$  as the excess  $Mg^{2+}$  in the RNA ion atmosphere increases. Putrescine<sup>2+</sup> is even more effective in competing  $Mg^{2+}$  from the extended conformation, independent of the  $Mg^{2+}$  excess. To account for these and other results, we propose that both ions closely approach the surface of RNA secondary structure, but the completely folded RNA tertiary structure develops small pockets of very negative electrostatic potential that are more accessible to the compact charge of  $Mg^{2+}$ . The sensitivity of RNA folding to the combination of  $Mg^{2+}$  and putrescine<sup>2+</sup> found *in vivo* depends on the architectures of both the unfolded and native conformations.

## INTRODUCTION

It is well-known that most of the negative charge of an RNA in solution is compensated by the accumulation of excess cations in its vicinity, with only a small fraction of the phosphate charges balanced by the nearby depletion of mobile anions (1,2). The identity of the cation may strongly influence the folding equilibrium of an RNA: moderate concentrations of  $K^+$  stabilize many RNAs in their native structure (3), but it has been known for 40 years that  $Mg^{2+}$  promotes RNA folding far more effectively, even in the presence of

the large excess of monovalent ions present *in vivo* (4). One reason  $Mg^{2+}$  is so effective is the entropic advantage of its divalent charge, which allows the same amount of positive charge to be positioned near an RNA with half the number of particles needed with monovalent ions; the energetic advantage is larger for RNAs with more compact structures that tend to concentrate cations closer to their surfaces (5). Another consideration is that  $Mg^{2+}$  is generally more effective at stabilizing RNA tertiary structure than larger group II cations, in part because its small size allows it to accumulate closer to the convoluted surfaces of RNAs tertiary structures (6–8).

Among divalent cations that stabilize RNA tertiary structures, of particular relevance is putrescine<sup>2+</sup>, which is abundant in bacteria. The total cellular putrescine<sup>2+</sup> concentration varies as much as 8-fold in response to changes in growth conditions and may approach the total  $Mg^{2+}$  concentration in *Escherichia coli* (9,10); the ion is probably essential for optimum translation rates and cell growth (11–13). We previously found that some RNA tertiary structures are stabilized by putrescine<sup>2+</sup>, though not as effectively as by  $Mg^{2+}$ ; it is possible that putrescine<sup>2+</sup> contributes a small additional stability to these RNAs at concentrations of  $Mg^{2+}$  and putrescine<sup>2+</sup> found *in vivo* (14). Putrescine<sup>2+</sup> acts very differently with a class of RNA structures that are known to chelate  $Mg^{2+}$ ; these RNAs are slightly destabilized by putrescine<sup>2+</sup>, again at  $Mg^{2+}$  and putrescine<sup>2+</sup> concentrations comparable to those found *in vivo* (14). These observations underscore the importance of extending RNA folding studies to include putrescine<sup>2+</sup> as well as  $Mg^{2+}$  and  $K^+$ .

A simple thermodynamic cycle illustrates how the stability of an RNA structure is affected by the strength of ion interactions with both the folded and unfolded forms of the RNA (Figure 1A). Thus, to understand the differing responses of RNA tertiary structures to  $Mg^{2+}$  and putrescine<sup>2+</sup>, it is necessary to know how effectively the two ions compete with each other for interactions with both extended and compact conformations of an RNA. In this work, we examine  $Mg^{2+}$ –putrescine<sup>2+</sup> competition

\*To whom correspondence should be addressed. Tel: +1 503 583 0094; Fax: +1 410 516 8420; Email: draper@jhu.edu

Present address: R. J. Trachman, III, Biochemistry and Biophysics Center, National Heart, Lung and Blood Institute, National Institutes of Health, Bethesda, MD 20814, USA.

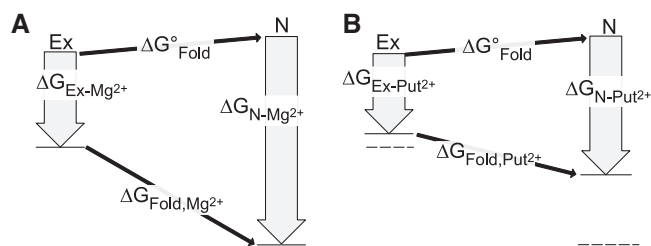


**Figure 1.** Thermodynamic cycles showing the relation between ion–RNA interaction strengths with partially unfolded (here the ‘extended’ conformation, Ex) and native (N) RNA conformations and overall RNA stability. The diagram assumes initial standard conditions of monovalent ions and temperature such that the RNA folding is unfavorable ( $\Delta G^\circ_{\text{Fold}} > 0$ ). (A)  $\text{Mg}^{2+}$  interacts more strongly with the N conformation than with Ex, resulting in a stabilization of the native structure and a favorable free energy of folding. (B) Putrescine $^{2+}$  interacts more weakly than  $\text{Mg}^{2+}$  with both the Ex and N conformations. (Dashed lines correspond to arrow positions from panel A.) Although the weakening is more pronounced with the N state, at high enough concentrations putrescine $^{2+}$  is still able to induce folding. The sizes of the vertical arrows are meant as a qualitative illustration, and are not to scale for the A-riboswitch.

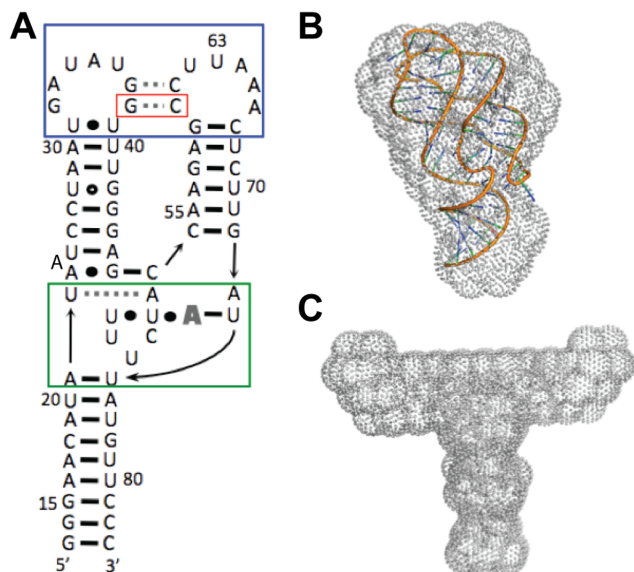


**Figure 2.** Structure of the adenine riboswitch. (A) secondary structure. Arrows denote 5′–3′ backbone connectivity; horizontal black bars represent Watson–Crick base pairing; black dots represent non-canonical pairing; and dashed lines indicate base–base tertiary interactions. There are two sets of tertiary interactions, the ‘kissing loop’ (blue box) and ligand binding pocket (green box, adenine ligand in bold). The tertiary pair disrupted by the C60G mutation is boxed in red. (B) Reconstruction of the native A-riboswitch structure calculated from SAXS data in the presence of DAP ligand and 10 mM putrescine $^{2+}$ ; the reconstructed scattering density (gray spheres) is superimposed on an A-riboswitch crystal structure (1Y26). (C) Reconstruction of the C60G A-riboswitch scattering density in the presence of 2 mM putrescine $^{2+}$  and absence of ligand. Two-fold symmetry has been imposed in the calculation (see Materials and Methods).

for interactions with the adenine riboswitch aptamer (Figure 2) when it is in either its compact, native conformation or in an extended, partially unfolded form. We use a titration method that allows us to assess the total free energy of  $\text{Mg}^{2+}$ –RNA interactions in the presence of increasing concentrations of competing putrescine $^{2+}$  (15). We find that putrescine $^{2+}$  is most effective as a competitor when the

RNA is largely secondary structure, becomes less effective as the RNA becomes more compact, and is an extremely weak competitor when  $\text{Mg}^{2+}$  interacts primarily with the one or two regions where RNA phosphates are brought closest together by the RNA tertiary structure.

The idea that  $\text{Mg}^{2+}$  plays a special role in RNA folding because of its access to small pockets of negative charge created by tertiary structures was proposed in early studies with tRNA (4,16) and supported by later electrostatic computations (17). Subsequent quantitative measurements of  $\text{Mg}^{2+}$ –RNA interaction free energies have recently been useful benchmarks for more sophisticated computational studies of the distribution of  $\text{Mg}^{2+}$  near an RNA tertiary structure (18,19). The present data add to this developing picture by providing quantitative free energy measurements of two divalent ions competing for interactions with different RNA conformations, and are relevant to the more complex *in vivo* environment where RNA functions in the presence of multiple kinds of cations.

## MATERIALS AND METHODS

### Preparation of solutions and RNA

All solutions were prepared using water at 18.3 M $\Omega$  resistivity. All buffers and salts were  $\geq 99.5\%$  purity. MOPS buffer was obtained from Sigma, and brought to pH 6.8 with KOH (K•MOPS). The standard buffer was 40 mM K•MOPS (with 13 mM  $\text{K}^+$ ), 10  $\mu\text{M}$  ethylenediaminetetraacetic acid (EDTA) (Sigma) and 37 mM KCl (Fluka) to give a total  $\text{K}^+$  concentration of 50 mM.  $\text{MgCl}_2$  and/or diamine were also added as indicated. The first acid dissociation constant of putrescine is  $\text{pK}_a = 9.36$  (14); thus, at pH 6.8 more than 99% of the putrescine is the di-protonated species. Solutions of  $\text{MgCl}_2$  (Fluka) were standardized by titration into an EDTA solution (pH 8.0) of known concentration, while monitoring absorbance at 230 nm (20). 8-hydroxyquinoline sulfonic acid (HQS, Sigma Chemicals) was purified by recrystallization as described (20).

All RNAs were prepared by transcription of linearized plasmid DNA with a hexa-histidine-tagged bacteriophage T7 RNA polymerase; the plasmids have been described previously (21,22). Transcription products were purified by preparative electrophoresis on denaturing, 12% polyacrylamide gels. The desired product band was excised from the gel, from which the RNA was electroeluted in an Elu-trap Electrophoresis Chamber (Schleicher & Schuell). Centricon filter units (Millipore) with a 3K molecular weight cutoff were used to equilibrate RNA to the desired buffer. An excess of a high-affinity ligand for the A-riboswitch, 2,6-diaminopurine (DAP), was used to maintain the RNA in its native conformation (22).

### Measurement of excess $\text{Mg}^{2+}$

The excess  $\text{Mg}^{2+}$  that neutralizes RNA charge,  $\Gamma_{\text{Mg}^{2+}}$ , is defined below (Background). It was measured by titration of  $\text{MgCl}_2$  into RNA solutions that contained HQS as a fluorescent reporter of bulk  $\text{Mg}^{2+}$  concentration. RNA samples for HQS titrations were dialyzed against a given concentration of putrescine $^{2+}$ , which is therefore the bulk con-

centration of putrescine<sup>2+</sup> as reported in the legend to Figure 3. (The total putrescine<sup>2+</sup> concentration will be higher than the bulk, because of putrescine<sup>2+</sup> interactions with the RNA.) The titrant of these experiments contained the standard buffer described above (40 mM K•MOPS pH 6.8, 37 mM KCl, 10 μM EDTA, for a total of 50 mM K<sup>+</sup>) with 20 mM MgCl<sub>2</sub> and the given putrescine<sup>2+</sup> concentration.

Two cuvettes with either dialyzed RNA sample or the dialysis buffer alone were titrated in an Aviv ATF 105 fluorometer outfitted with Hamilton automatic titrators. Both cuvettes contained 20 μM HQS; RNA samples were 2–4 mM in phosphate concentration. Reported titration curves are the averages of three to five experiments. The larger error bars for the ensemble RNA titrations are due to the smaller number of titrations (three) and larger variability between runs compared to the others, possibly related to the RNA conformation changes taking place during the titration. Data collection and analysis have been described in detail (20).

### X-ray scattering

RNA samples (1–2 mg/ml) were exchanged extensively into standard buffer (described above) with 0–50 mM putrescine•(HCl)<sub>2</sub> as indicated. The samples were heated to 65°C for 5 min and incubated at room temperature for at least 30 min. Samples were then passed through a 0.1 μm filter (Millipore) prior to beam exposure. SAXS measurements were performed at beamline 12-ID at the Advanced Photon Source, Argonne National Laboratory. The beam energy was set to 12 keV with an exposure time of 0.5 s. Samples were moved through an X-ray flow cell to minimize radiation damage. The ambient temperature was ~25°C. Thirty shots were collected for each sample condition in order to obtain good statistics. Radii of gyration ( $R_g$ s) were determined from the Guinier fit to averaged data; P(r) plots were generated using GNOM after finding approximate  $D_{Max}$  values in AUTOGNOM (23). Envelopes were generated for the N and Ex-state using DAMMIF. The results of the simulated annealing procedure were uninterrupted for the Ex-state mutant in normal P1 mode, and the simulation was therefore rerun with P2 symmetry imposed.

### UV titrations

UV absorbance titrations were carried out in an Aviv 14-DS spectrophotometer. Titrations were carried out either with a Hamilton automatic titrator or by manual titrations while observing the 260 and 280 nm wavelengths. The results of both methods were identical. The initial absorbance of each sample was ~0.6 OD at 260 nm. The data were normalized to 1 by dividing the absorbance at a given concentration of divalent ion by the initial absorbance in the absence of divalent ion. Resulting titrations were fit to the Hill equation with the Hill coefficient and fractional change in OD as variables.

### BACKGROUND

The method we use here to measure the excess Mg<sup>2+</sup> accumulated by an RNA is based on the same principle as an

equilibrium dialysis experiment, in which an RNA solution is kept separate from buffer solution by a membrane permeable only to ions and water. Comparison of the concentrations of a particular cation or anion in the RNA solution ('in') and buffer only solution ('out') approximates the preferential interaction coefficient for that ion,

$$\Gamma_{Ion} = \frac{C_{Ion}^{In} - C_{Ion}^{Out}}{C_{RNA}} \approx \left( \frac{\partial C_{Ion}}{\partial C_{RNA}} \right)_{\mu_{Ion}} \quad (1)$$

where the chemical potential of the ion,  $\mu_{Ion}$ , must be identical on both sides of the membrane at thermodynamic equilibrium. Positive  $\Gamma_{Ion}$  values are called the *excess* of a particular cation; negative values are characteristic of an anion deficiency. The value of  $\Gamma_{Ion}$  measured by equilibrium dialysis or equivalent means (see Materials and Methods) can be an excellent approximation of the Equation (1) partial derivative that defines  $\Gamma_{Ion}$  (20). A more detailed yet accessible discussion of the meaning of  $\Gamma_{Ion}$  is in reference (24).

For an RNA with Z phosphate negative charges in a solution with the chloride salts of K<sup>+</sup>, Mg<sup>2+</sup> and putrescine<sup>2+</sup>, electroneutrality of the system requires the following relation between the interaction coefficients of the ions:

$$Z = 2\Gamma_{Mg^{2+}} + 2\Gamma_{Put^{2+}} + \Gamma_{K^+} + \Gamma_{Cl^-} \quad (2)$$

If the chemical potential of one of the ionic species in solution is changed, the system will equilibrate accordingly. For instance if the chemical potential of putrescine<sup>2+</sup> is increased,  $\Gamma_{Put^{2+}}$  will increase while  $\Gamma_{Mg^{2+}}$ ,  $\Gamma_{K^+}$  and  $\Gamma_{Cl^-}$  change in a compensatory fashion. A change in RNA conformation may also induce a set of compensatory changes among the  $\Gamma_{Ion}$  terms.

In this paper, we use the term 'ion exchange' to refer to the complete set of compensatory changes among the four  $\Gamma_{Ion}$  terms of Equation (2) in response to the change in chemical potential of one ionic species. Alternatively, we will refer to a reduction in  $\Gamma_{Mg^{2+}}$  caused by an increase in the concentration of putrescine<sup>2+</sup> as a 'competition' between the two divalent ions. Neither 'exchange' or 'competition' is meant to imply that putrescine<sup>2+</sup> and Mg<sup>2+</sup> are vying for a fixed number of specific 'sites', or that competition occurs only if one ion replaces another at a specific location. In fact, the long-range electrostatic interactions that define ion interactions with RNA couple ion interactions in such a way that an ion chelated at a specific site may be displaced by mobile ions within the ion atmosphere (25).

The partial derivative defining  $\Gamma_{Ion}$  (Equation (1)) can be transformed into an integral that gives the free energy of ion – RNA interactions. For Mg<sup>2+</sup>, this free energy is (15)

$$\Delta G_{RNA-Mg^{2+}} \approx -RT \int_0^{C_{Mg^{2+}}} \Gamma_{Mg^{2+}} d \ln C_{Mg^{2+}}. \quad (3)$$

When MgCl<sub>2</sub> is titrated into RNA in the presence of a large enough excess of KCl, the total Cl<sup>-</sup> concentration does not change significantly; thus  $\Delta G_{RNA-Mg^{2+}}$  can be obtained independently of the free energy of RNA – anion interactions.

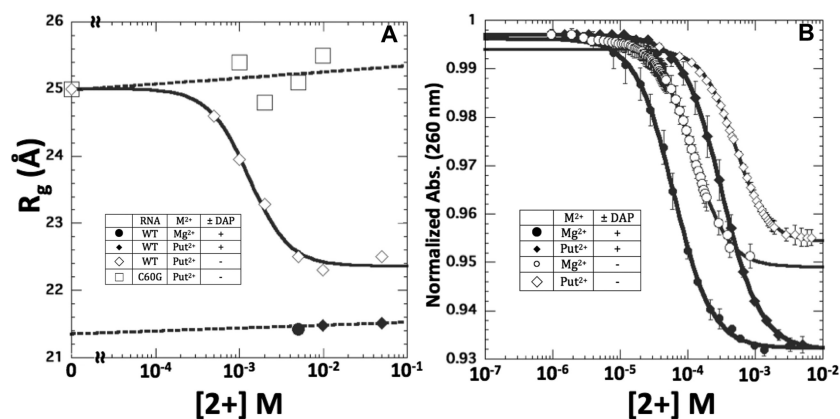


**Figure 3.** Effects of divalent ions on A-riboswitch folding. (A) Radius of gyration ( $R_g$ ) of the A-riboswitch in the presence and absence of 2,6-diaminopurine in varying concentrations of putrescine $^{2+}$  and  $Mg^{2+}$ . Also shown is  $R_g$  for C60G RNA titrated with putrescine $^{2+}$  (squares). (B) UV absorbance at 260 nm of the A-riboswitch in the presence and absence of ligand (DAP) in varying concentrations of putrescine $^{2+}$  and  $Mg^{2+}$ . Titration data in the two panels have been fit either to the Hill equation (solid curves) or a straight line (dashed).

## RESULTS

### Characterization of folded and extended adenine riboswitch conformations

The RNA used in these studies is a modified form of the aptamer domain of the *add* adenine riboswitch (A-riboswitch), an exceptional system for probing the details of RNA folding (26) (Figure 1A). (In conjunction with its expression platform, the aptamer domain regulates translation of a gene product responsible for adenine metabolism (27).) In the presence of adenine or select purine derivatives, the RNA folds to a compact tertiary structure in which the ligand is completely surrounded by the binding pocket and the two hairpin loops are docked in a kissing interaction (28). In the absence of both ligand and  $Mg^{2+}$ , the two hairpin loops tend to undock and the RNA samples extended conformations (29). Both ligand and  $Mg^{2+}$  favors docking of the hairpin loops, and together act synergistically to stabilize the native state (22,29,30). The strength of the kissing loop interaction varies with the exact sequence of the riboswitch (31,32); in the extreme case of the disruptive mutation C60G (29), the RNA folding equilibrium heavily favors an extended, T-shaped conformation even at moderate  $Mg^{2+}$  concentrations ((22) and Figure 2B, C). Over the range 0–0.1 mM  $Mg^{2+}$ , SAXS experiments found that the native (N state) structure is adopted by the Figure 2A A-riboswitch sequence when high ligand concentration is present, and an extended conformation (Ex state) by the C60G variant in the absence of ligand (22).

We first used SAXS and UV hypochromicity experiments to examine the effect of putrescine $^{2+}$  on the A-riboswitch and its C60G variant (Figure 3). The radius of gyration ( $R_g$ ) as measured by SAXS is primarily sensitive to the overall dimensions of a macromolecule; there is an easily detectable decrease ( $\sim 15\%$ ) in A-riboswitch  $R_g$  in going from the Ex to N states. Previous experiments showed that the A-riboswitch approaches the same  $R_g$  with or without ligand present, as  $Mg^{2+}$  is added to 1 mM (22). Putrescine $^{2+}$  is apparently less effective, as the reduction in  $R_g$  appears to plateau at  $\sim 80\%$  of the compaction seen in the pres-

ence of ligand (Figure 3A). (The  $P(r)$  distribution of the A-riboswitch with putrescine $^{2+}$  is also subtly different from that found with  $Mg^{2+}$ , Supplementary Figure S1A.) A potential caveat is that concentrations of putrescine $^{2+} > \sim 10$  mM significantly increase the concentration of  $Cl^-$  beyond the 50 mM already present with KCl, which could change  $\Gamma_{Cl^-}$  during the titration with unknown effects on other  $\Gamma_{Ion}$  and the docking equilibrium. However, UV absorption experiments (described below) suggest the plateau is not an artifact.

Two additional results from the SAXS experiments are important for interpretation of the  $\Gamma_{Mg^{2+}}$  measurements that follow. First, with A-riboswitch in the presence of ligand, putrescine $^{2+}$  does not alter either the native structure  $R_g$  (Figure 3A) or distance distribution profile ( $P(r)$ , Supplementary Figure S1C) from that observed with  $Mg^{2+}$ . Second, C60G RNA remains in an extended conformation at high putrescine $^{2+}$  concentrations (Figure 3A, Supplementary Figure S1B), as previously observed with  $Mg^{2+}$  (22). Thus, at the level of resolution available from SAXS experiments, putrescine $^{2+}$  and  $Mg^{2+}$  do not alter the N or Ex state structures within the ion concentration ranges used in our studies. It is not critical for this study whether C60G RNA is rigidly fixed in an extended conformation; some flexibility is suggested by the fact that high divalent ion concentrations drive it into a somewhat more compact conformation. The important conclusion for our competition experiments is that, within the ionic concentration range used here, C60G RNA maintains a constant  $R_g$  approximately that of unfolded A-riboswitch RNA in the absence of both divalent ions and ligand.

UV absorption is sensitive to base stacking in RNA, and in the A-riboswitch hypochromicity associated with folding likely originates from structures formed within both the docked loops and the binding pocket. In the presence of ligand, putrescine $^{2+}$  and  $Mg^{2+}$  titrate  $A_{260}$  to the same endpoints (Figure 3B). A smaller hyperchromic change is seen in the absence of ligand when either divalent ion is present, possibly because the binding pocket does not become fully structured. Putrescine $^{2+}$  induces marginally less

hyperchromicity than does  $\text{Mg}^{2+}$ , but the titration curve notably approaches a plateau at less than 10 mM putrescine $^{2+}$ . This endpoint suggests the apparent plateau of the SAXS titration curve is not an artifact of increasing  $\text{Cl}^-$  concentration, and that putrescine $^{2+}$  in the absence of ligand stabilizes an RNA conformation in which the hairpin loops occupy an intermediate position between that of the docked native structure and the fully extended loop-loop configuration.

We conclude from these experiments that  $\Gamma_{\text{Mg}^{2+}}$  can be calculated by Equation (3) for the A-riboswitch RNA–ligand complex and for the variant C60G RNA when ions are varied from 0 to  $\sim 10$  mM putrescine $^{2+}$  and 0 to  $\sim 0.1$  mM  $\text{Mg}^{2+}$ . In the absence of ligand, the A-riboswitch RNA undergoes a significant shift in dimensions over the same ranges of concentrations, and Equation (3) is not applicable.

### Measurement of excess $\text{Mg}^{2+}$ upon addition of putrescine $^{2+}$

To study the effect of putrescine $^{2+}$  on  $\text{Mg}^{2+}$ –A-riboswitch interactions, we quantified excess  $\text{Mg}^{2+}$  ions accumulated by the RNA during titrations in the presence of a fluorescent  $\text{Mg}^{2+}$  chelator, HQS (see Materials and Methods). Titrations were carried out in the presence of fixed concentrations of putrescine $^{2+}$ , with either wild-type A-riboswitch in the presence of ligand (Native state, Figure 2B) or the C60G variant without ligand (Extended state, Figure 2C). A third set of titrations was made with A-riboswitch RNA without ligand, which permits a partial folding transition as divalent ions are titrated (compare SAXS and UV titrations in the absence of ligand, Figure 3). We refer to RNA under these conditions as ‘ensemble’ RNA, because it may adopt multiple conformations.

The titration curves show that increasing putrescine $^{2+}$  concentration for any of the three conditions results in a net decrease in  $\Gamma_{\text{Mg}^{2+}}$  over the entire curve, which implies that excess putrescine $^{2+}$  accumulates at the expense of excess  $\text{Mg}^{2+}$  (Equation (2)). As observed previously (22),  $\Gamma_{\text{Mg}^{2+}}$  depends on the dimensions of the RNA with the more compact form (N state) possessing a larger  $\Gamma_{\text{Mg}^{2+}}$  than the less compact Ex state (Figure 4A and B); this difference holds true when putrescine $^{2+}$  is present. However, the relative decrease in  $\Gamma_{\text{Mg}^{2+}}$  caused by putrescine $^{2+}$  tends to be much greater for the Ex state. For instance 10 mM putrescine $^{2+}$  reduces  $\Gamma_{\text{Mg}^{2+}}$  at 0.1 mM  $\text{Mg}^{2+}$  by  $\sim 55\%$  (to  $\sim 3.6$  ions/RNA) for the N state, but by over 80% for the Ex state (to  $\sim 1$  ion/RNA).  $\Gamma_{\text{Mg}^{2+}}$  for the ensemble RNA generally lies between values found for the N and Ex states as illustrated for the titrations with 5 mM putrescine $^{2+}$  (Figure 4D): the ensemble curve is similar to that of the Ex state at low  $C_{\text{Mg}^{2+}}$ , but rises toward the N state curve at higher  $C_{\text{Mg}^{2+}}$ .

### Free energies of RNA– $\text{Mg}^{2+}$ interaction

By integrating the  $\Gamma_{\text{Mg}^{2+}}$  curves in Figure 4A and B, RNA– $\text{Mg}^{2+}$  interaction free energy values ( $\Delta G_{\text{RNA-Mg}^{2+}}$ , as defined in Figure 1A) are obtained per Equation (3) (Figure 5). (Only the curves for the N and Ex state titra-

tions provide reliable  $\Delta G_{\text{RNA-Mg}^{2+}}$  values, since these structures are unchanged during the titration.) We see approximately linear decreases in  $\Delta G_{\text{N-Mg}^{2+}}$  and  $\Delta G_{\text{Ex-Mg}^{2+}}$  with the log of the putrescine $^{2+}$  concentration, though with different slopes:  $\Delta G_{\text{Ex-Mg}^{2+}}$  is more sensitive to the addition of putrescine $^{2+}$ . The difference between these free energies,  $\Delta\Delta G = \Delta G_{\text{N-Mg}^{2+}} - \Delta G_{\text{Ex-Mg}^{2+}}$ , would be the contribution of  $\text{Mg}^{2+}$  to the stability of an Ex  $\rightarrow$  N folding transition, and should increase in magnitude as the putrescine $^{2+}$  concentration increases. (See the thermodynamic cycle, Figure 1A.) Because  $\Delta G_{\text{RNA-Mg}^{2+}}$  is directly related to  $\Gamma_{\text{Mg}^{2+}}$ , another way to visualize this observation is that the number of  $\text{Mg}^{2+}$  ions taken up in an Ex  $\rightarrow$  N transition,  $\Delta\Gamma_{\text{Mg}^{2+}}$ , should increase upon putrescine $^{2+}$  addition despite the fact that putrescine $^{2+}$  decreases  $\Gamma_{\text{Mg}^{2+}}$  for both states of the RNA. (Note that an Ex  $\rightarrow$  N transition is hypothetical: in the absence of the C60G mutation to enforce an extended conformation, A-riboswitch RNA tends to adopt more compact conformations when titrated with  $\text{Mg}^{2+}$ , and thus reduce  $\Delta\Gamma_{\text{Mg}^{2+}}$ .)

Although the free energy of  $\text{Mg}^{2+}$  interaction with ensemble RNA cannot be calculated, the effects of putrescine $^{2+}$  addition on  $\Gamma_{\text{Mg}^{2+}}$  of N, Ex and ensemble RNAs can be compared; Supplementary Figure S2 shows how rapidly  $\Gamma_{\text{Mg}^{2+}}$  decreases with increasing putrescine $^{2+}$  concentration while  $C_{\text{Mg}^{2+}}$  is held constant. The ensemble RNA resembles Ex RNA in its sensitivity to putrescine $^{2+}$  at a lower  $C_{\text{Mg}^{2+}}$  (Supplementary Figure S2B) and is midway between N and Ex RNAs at a higher  $C_{\text{Mg}^{2+}}$  that induces a small degree of compaction in A-riboswitch RNA in the absence of ligand (Supplementary Figure S2A and (22)).

### $\text{Mg}^{2+}$ –putrescine $^{2+}$ exchange at constant $\Gamma_{\text{Mg}^{2+}}$

An alternative perspective on the competition between  $\text{Mg}^{2+}$  and putrescine $^{2+}$  is suggested by the horizontal line in Figure 4 panels A and B, drawn for  $\Gamma_{\text{Mg}^{2+}} = 1.0$ . The intersections of this line with the successive titration curves at increasing concentrations of putrescine $^{2+}$  ask: if a given amount of putrescine $^{2+}$  is added to a system with an initial  $\Gamma_{\text{Mg}^{2+}}$ , how much  $\text{Mg}^{2+}$  must also be added in order to return to the same value of  $\Gamma_{\text{Mg}^{2+}}$ ? It is helpful to view the ion concentrations in terms of chemical potentials, where for two solutions with different ion concentrations

$$\Delta\mu_{\text{Mg}^{2+}} = \mu_{\text{Mg}^{2+},2} - \mu_{\text{Mg}^{2+},1} \approx -RT \ln(C_{\text{Mg}^{2+},2}/C_{\text{Mg}^{2+},1}) \quad (4)$$

and a similar relation holds for  $\Delta\mu_{\text{Put}^{2+}}$ . (The activity coefficients of divalent ions in a solution of excess KCl are relatively insensitive to the overall  $\text{MgCl}_2$  or putrescine $\bullet\text{Cl}_2$  concentration; hence the activity coefficients should approximately cancel and have been omitted in Equation (4).) The plots in Figure 6A shows that there is an approximately linear relation between the two chemical potential changes needed to keep  $\Gamma_{\text{Mg}^{2+}}$  constant, i.e.

$$\Delta\mu_{\text{Mg}^{2+}} = m\Delta\mu_{\text{Put}^{2+}} \quad (5)$$

where  $m$  is the slope of the plots. For the Ex state,  $m \approx 1$ : a given increase in  $\mu_{\text{Mg}^{2+}}$  is countered by an equivalent in-

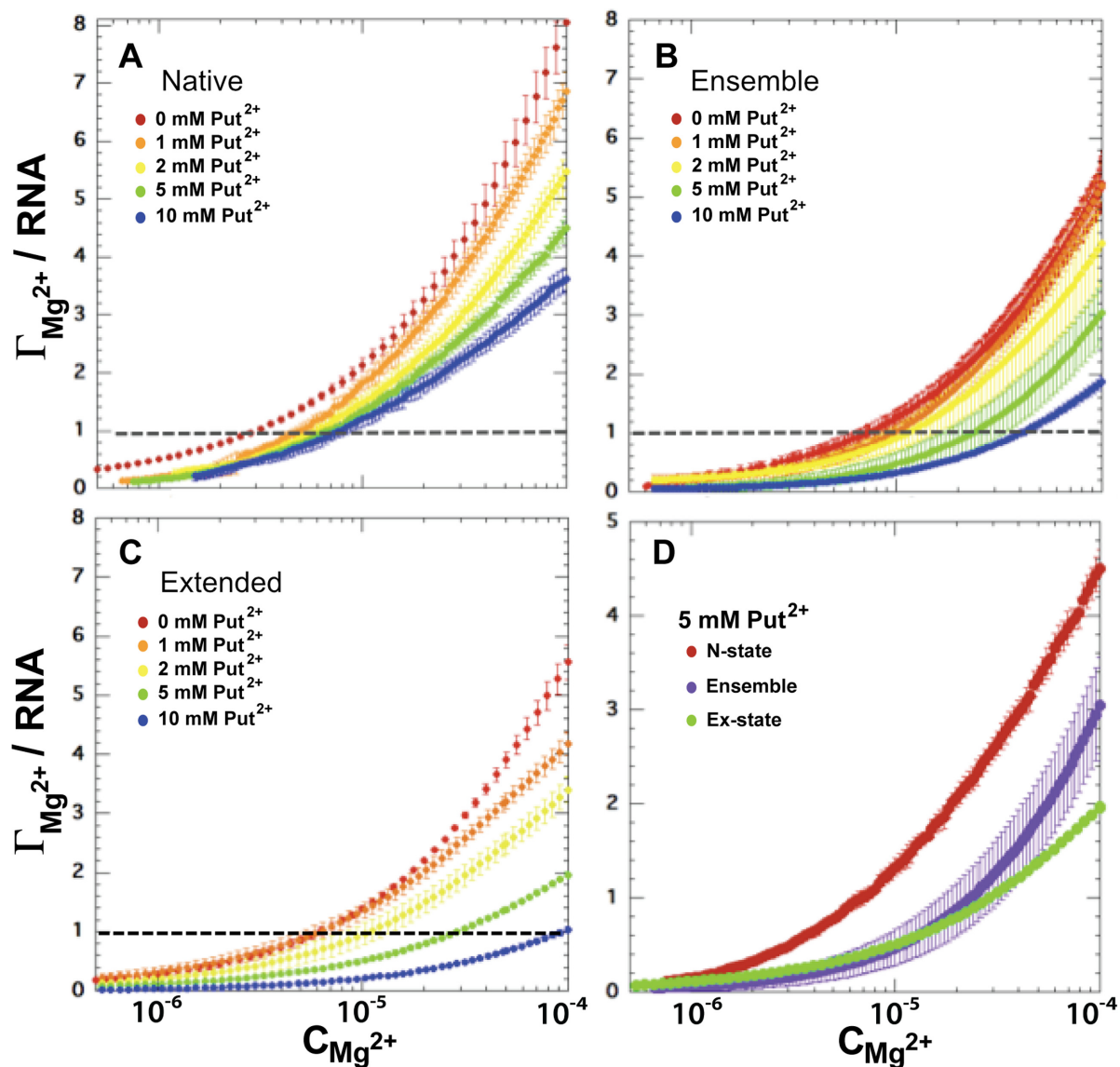


**Figure 4.**  $\text{Mg}^{2+}$  titrations in the presence of the fluorophore HQS. (A–C) Excess  $\text{Mg}^{2+}$  ( $\Gamma_{\text{Mg}^{2+}}$ ) as a function of bulk  $\text{Mg}^{2+}$  concentration ( $C_{\text{Mg}^{2+}}$ ) of the A-riboswitch that had been dialyzed against putrescine $^{2+}$  concentrations from 0 to 10 mM. (A) N state A-riboswitch in the presence of 250  $\mu\text{M}$  2,6-diaminopurine. (B) A-riboswitch in the absence of ligand. (C) Ex state (C60G) mutant. (D) Curves for the N-state A-riboswitch (red), A-riboswitch without ligand (purple) and Ex state (C60G mutant, green) in the presence of 5 mM putrescine $^{2+}$ . The dashed line in panels A and B indicates the constant value of  $\Gamma_{\text{Mg}^{2+}}$  used to prepare Figure 5A.

crease in  $\mu_{\text{Put}^{2+}}$ . However, putrescine $^{2+}$  is much less effective at displacing  $\text{Mg}^{2+}$  from the N state excess ions:  $m \approx 0.2$ , and a given increase in  $\mu_{\text{Mg}^{2+}}$  requires a five fold larger increase in  $\mu_{\text{Put}^{2+}}$  to maintain constant  $\Gamma_{\text{Mg}^{2+}}$ . With ensemble RNA,  $m \approx 0.65$  is intermediate between N and Ex state RNAs. Not only do putrescine $^{2+}$  and  $\text{Mg}^{2+}$  compete against each other as  $\mu_{\text{Mg}^{2+}}$  and  $\mu_{\text{Put}^{2+}}$  increase, but the increase in total divalent ion concentration presumably decreases  $\Gamma_{\text{K}^+}$  and possibly also  $-\Gamma_{\text{Cl}^-}$ , to establish a final set of  $\Gamma_{\text{Ion}}$  that satisfy Equation (2). Although a complete determination of all four  $\Gamma_{\text{Ion}}$  from the Figure 5 data are not possible, the Figure 6A plot provides a simple quantitation of the efficiency with which putrescine $^{2+}$  ions ‘exchange’ with other excess ions of an RNA. Qualitatively, the plot suggests that ion

exchange is much more efficient with more extended RNA conformations. (Note that  $m$  should be taken only as a *relative* measure of ion exchange efficiency; without knowing all four  $\Gamma_{\text{Ion}}$  values, we cannot interpret the absolute value of  $m$ . In particular,  $m$  is not a simple stoichiometric ratio: e.g.,  $m = 1$  does not imply that one putrescine $^{2+}$  replaces one  $\text{Mg}^{2+}$ .)

A further point, revealed by Figure 6B, is that  $m$  for the N state increases substantially as the constant value of  $\Gamma_{\text{Mg}^{2+}}$  is raised, reaching  $\sim 0.6$  when  $\Gamma_{\text{Mg}^{2+}} = 3.6$  ions/RNA. Thus, putrescine $^{2+}$  becomes a progressively more effective replacement for  $\text{Mg}^{2+}$  as the number of excess  $\text{Mg}^{2+}$  increases. Although  $m$  values for Ex and ensemble state RNAs are available over only a limited range of  $\Gamma_{\text{Mg}^{2+}}$  values, it appears

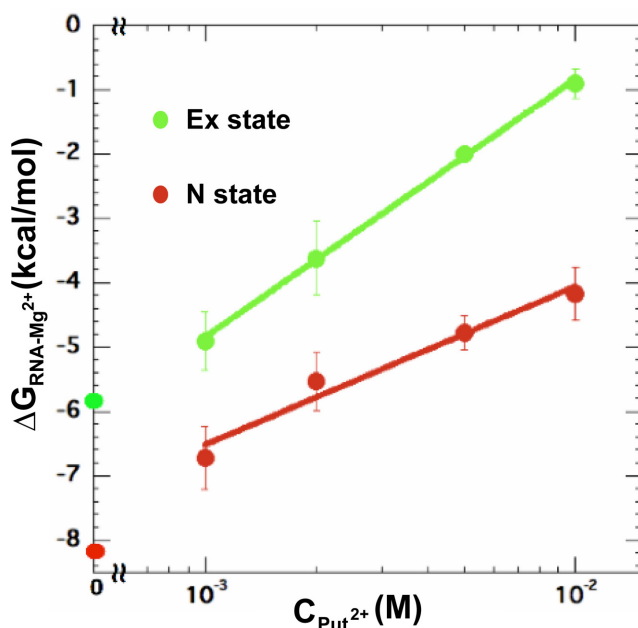


**Figure 5.** The RNA-Mg<sup>2+</sup> interaction free energy calculated at 0.1 mM Mg<sup>2+</sup> as a function of bulk putrescine<sup>2+</sup> concentration for the N and Ex states. Points on the y-axis are  $\Delta G_{\text{RNA-Mg}^{2+}}$  values in the absence of putrescine<sup>2+</sup>.

that  $m$  is approximately constant with these more extended RNA conformations (Figure 6C). (Note that the maximum values of  $\Gamma_{\text{Mg}^{2+}}$  in Figure 6C are low, with <10% of the A-riboswitch phosphates neutralized by excess Mg<sup>2+</sup>. The trends observed in these plots may well diverge at much higher  $\Gamma_{\text{Mg}^{2+}}$ .) These results are interpreted in the Discussion in terms of the interaction free energies available to putrescine<sup>2+</sup> and Mg<sup>2+</sup> near different types of RNA surfaces.

## DISCUSSION

### Divalent ion–RNA interactions

One of the main driving forces of RNA tertiary folding is the uptake of cations that accompanies the transition from an extended, partially structured conformation to the compact native structure. It is well established that divalent ions are taken up in strong preference to monovalent ions (4,33,34), and Mg<sup>2+</sup> is generally a more potent stabilizer of RNA tertiary folds than larger group II ions or divalent organic ions (6,35–38). In this study, by quantifying Mg<sup>2+</sup> and putrescine<sup>2+</sup> interactions with RNAs in defined conformational states we show why putrescine<sup>2+</sup> tends to be much less stabilizing than Mg<sup>2+</sup>.

Since Mg<sup>2+</sup> and putrescine<sup>2+</sup> are drastically different in their overall size and shape, it is important to first note how those differences may influence their capacity to interact with RNA. A first consideration is the entropic advantage of divalent ions over monovalent. When Mg<sup>2+</sup> is added to a solution of RNA in monovalent ion, a single Mg<sup>2+</sup> replaces approximately two M<sup>+</sup> among the excess ions neutralizing RNA charge; the entropy of liberating two M<sup>+</sup> into the bulk solution outweighs the cost of localizing a single Mg<sup>2+</sup> to

a small volume surrounding the RNA (17). This entropic principle applies to putrescine<sup>2+</sup> as well as Mg<sup>2+</sup>.

A second factor to consider is the overall free energy of interaction between the divalent cations and the RNA ( $\Delta G_{\text{RNA-Mg}^{2+}}$  or  $\Delta G_{\text{RNA-Put}^{2+}}$ ), which is strongly electrostatic in origin: the most favorable free energies are developed when ions occupy regions of negative electrostatic potential created by several nearby phosphates. At one extreme, so-called ‘diffuse’ ions remain fully hydrated near or some distance from the RNA surface (43). At the other extreme, partially dehydrated Mg<sup>2+</sup> may make two or more direct contacts with the RNA in small pockets of concentrated negative charge, sometimes entirely buried within the solvent-accessible surface of the RNA (39–41). These ‘chelation’ sites cannot accommodate the elongated putrescine<sup>2+</sup> ion, and in fact RNAs with well-defined Mg<sup>2+</sup> chelation sites cannot be driven to adopt their native structure when putrescine<sup>2+</sup> is the sole divalent ion (14). Because putrescine<sup>2+</sup> does substitute for Mg<sup>2+</sup> in stabilizing the A-riboswitch native structure (14), and crystal structures of the A-riboswitch with resolved Mg<sup>2+</sup> have not revealed any chelated Mg<sup>2+</sup> (28,42), this special type of Mg<sup>2+</sup>–RNA interaction is unlikely to occur in the A-riboswitch.

Between the two extremes of chelated and diffuse ion interactions, ions may occupy regions within the first few hydration layers of the RNA where the energetics of the interaction are influenced by the ability of the ion to hydrogen bond to the RNA surface, directly or via the ion’s own hydration layer, and where the ion may be in close proximity to several phosphates. A recent crystal structure of the ribosome (44) suggests that putrescine<sup>2+</sup>, despite its size, may readily occupy locations at the RNA surface. Two putrescine<sup>2+</sup> ions are found in the major groove of A-form RNA segments, each with one amino group directly hydrogen bonded to a phosphate and the other 4–4.5 Å from a second phosphate (Supplementary Figure S3). In RNA crystal structures, Mg<sup>2+</sup> is frequently observed within A-helix major grooves with its first hydration layer hydrogen bonded to bases or phosphates (45,46). The estimated electrostatic potential within the groove is very negative (17,47), and a study that combined MD simulations with X-ray scattering data suggested that a large fraction of excess Mg<sup>2+</sup> accumulates deep in the RNA major groove (48). Thus, in the A-helix major groove, Mg<sup>2+</sup> and putrescine<sup>2+</sup> can position positive charge in similar locations at the RNA surface. Putrescine<sup>2+</sup> may also occupy pockets of negative charge associated with tertiary folding, as suggested by putrescine<sup>2+</sup> hydrogen-bonded to three phosphates brought into close proximity by the 23S rRNA tertiary structure (44).

### Competition between Mg<sup>2+</sup> and putrescine<sup>2+</sup>

Our previous study showed that about an order of magnitude higher concentration of putrescine<sup>2+</sup> than Mg<sup>2+</sup> is needed to induce folding of the A-riboswitch tertiary structure (14). The contribution of a divalent ion to the folding free energy is the difference in the ion interaction free energies between folded and unfolded RNA:  $\Delta\Delta G = \Delta G_{\text{N-Mg}^{2+}} - \Delta G_{\text{Ex-Mg}^{2+}}$ . Figure 1A implies that the weaker efficiency of putrescine<sup>2+</sup> could arise from many combinations of increases or decreases in  $\Delta G_{\text{Ex-Put}^{2+}}$  and  $\Delta G_{\text{N-Put}^{2+}}$  relative to

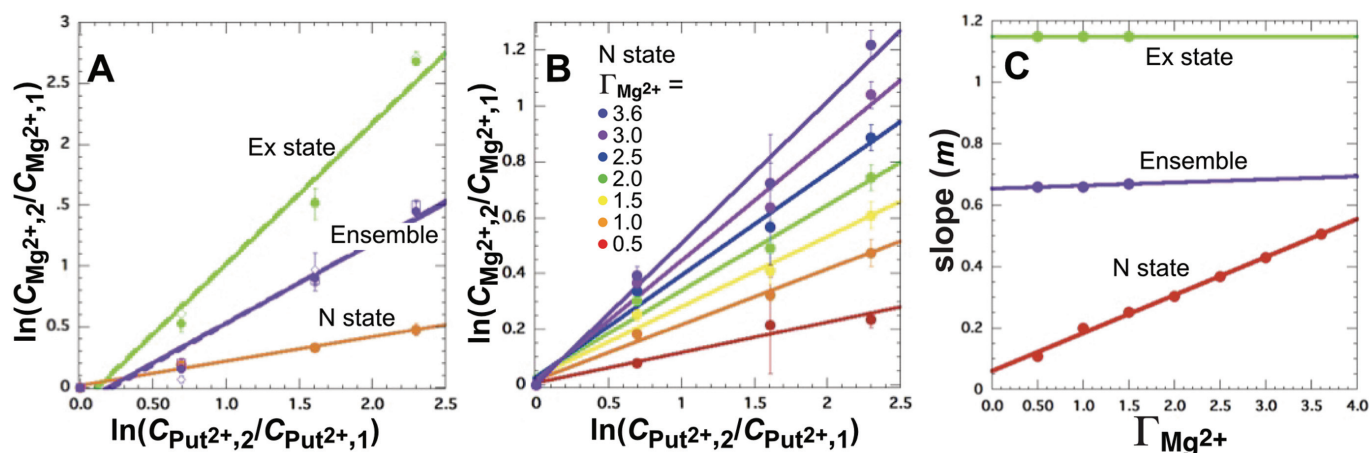


**Figure 6.** Coordinated changes in  $C_{\text{Mg}^{2+}}$  and  $C_{\text{Put}^{2+}}$  that maintain constant  $\Gamma_{\text{Mg}^{2+}}$ . The reference ion concentration  $C_{\text{Put}^{2+},1}$  is 1 mM;  $C_{\text{Mg}^{2+},1}$  is the concentration of  $\text{Mg}^{2+}$  needed to reach the given  $\Gamma_{\text{Mg}^{2+}}$  in the  $C_{\text{Put}^{2+}} = 1$  mM titration (Figure 4). (A) Plot of the change in  $C_{\text{Mg}^{2+}}$  versus change in  $C_{\text{Put}^{2+}}$  for the N state, Ex state and ensemble RNAs at constant  $\Gamma_{\text{Mg}^{2+}} = 1$  (solid lines, filled symbols) or  $\Gamma_{\text{Mg}^{2+}} = 0.5$  and 1.5 for the ensemble and Ex-state, respectively (open symbols and dashed lines, which nearly superimpose with the  $\Gamma_{\text{Mg}^{2+}} = 1$  data). (B) Native state at the indicated  $\Gamma_{\text{Mg}^{2+}}$ . (C) slope  $m$  (Equation (5)) taken from Figure 5A, B and additional data (not shown) as a function of  $\Gamma_{\text{Mg}^{2+}}$ . Lines are drawn for N state, Ex state and ensemble RNAs.

the corresponding  $\text{Mg}^{2+}$ –RNA interaction strengths. The ion titration data presented in this work (Figure 4, as interpreted in Figures 5, 6 and Supplementary Figure S2) reveal these differences in detail.

We first infer that  $\text{Mg}^{2+}$  develops a more favorable interaction free energy with the Ex state conformation than does putrescine $^{2+}$ , i.e.  $-\Delta G_{\text{Ex-Mg}^{2+}} > -\Delta G_{\text{Ex-Put}^{2+}}$ . For instance, a 20- to 30-fold excess of putrescine $^{2+}$  over  $\text{Mg}^{2+}$  is needed to halve  $-\Delta G_{\text{Ex-Mg}^{2+}}$  (Figure 5). The surface of Ex state RNA must be largely A-form helices; as discussed above both divalent ions may lie within the major groove, where electrostatic interactions are optimal. But  $-\Delta G_{\text{Ex-Put}^{2+}}$  includes not only a favorable electrostatic term, but also an entropic penalty for restricted motion of the putrescine $^{2+}$  butyl chain. The penalty could be more than 1 kcal/mol (14) and largely account for the weaker putrescine $^{2+}$  interactions. Indirect measurements of  $\text{Mg}^{2+}$  and putrescine $^{2+}$  interactions with helical DNA found that  $\text{Mg}^{2+}$  is favored by  $\sim -0.7$  kcal/mol (49), qualitatively consistent with the Ex state RNA results.

Turning to the N state RNA conformation, we first note that an even higher concentration of putrescine $^{2+}$  is needed to displace  $\text{Mg}^{2+}$  with this RNA than with the Ex state RNA, evidenced by both a lesser rate of decrease in  $-\Delta G_{\text{N-Mg}^{2+}}$  with increasing putrescine $^{2+}$  concentration (Figure 5), and a weaker effect on  $\Gamma_{\text{Mg}^{2+}}$  (Supplementary Figure S2). The reduced effectiveness of putrescine $^{2+}$  with the N state is doubtlessly linked to the formation of tertiary structures; both the ligand binding pocket and kissing loop (Figure 2A) contain closely spaced phosphates, which may create pockets of negative electrostatic potential that are more accessible to  $\text{Mg}^{2+}$  than putrescine $^{2+}$ . Evidence that putrescine $^{2+}$  might not be able to access some regions of the native tertiary structure as effectively as  $\text{Mg}^{2+}$  comes from the SAXS and UV hypochromicity observations that putrescine $^{2+}$ , without the help of ligand, does not fold the

RNA into a structure that is as compact as the one stabilized by  $\text{Mg}^{2+}$  (Figure 3).

As developed in Results, Equations (4) and (5),  $m$  is a measure of how hard the putrescine $^{2+}$  chemical potential has to ‘push’ against an increase in the  $\text{Mg}^{2+}$  chemical potential to keep  $\Gamma_{\text{Mg}^{2+}}$  constant. To interpret the way  $m$  increases with  $\Gamma_{\text{Mg}^{2+}}$  with the folded N state RNA (Figure 6C), we suppose that volumes near the surface of the native RNA exhibit a wide range of electrostatic potential, from smaller pockets of dense negative charge formed by the tertiary structure to larger volumes in the helix grooves with more widely spaced phosphates and less favorable interactions with cations. We further suppose that putrescine $^{2+}$  is unable to place positive charge within the smaller volumes with the most negative potential as effectively as  $\text{Mg}^{2+}$ , but that the two ions comes closer to parity within the more weakly interacting regions associated with secondary structure. Since  $\text{Mg}^{2+}$  will tend to first populate the small regions of most negative potential at low  $\Gamma_{\text{Mg}^{2+}}$  and appear more frequently around the secondary structure as  $\Gamma_{\text{Mg}^{2+}}$  increases, this simple model predicts that progressively smaller increases in  $\Delta\mu_{\text{Mg}^{2+}}$  will be needed to counter increases in  $\Delta\mu_{\text{Put}^{2+}}$  as  $\Gamma_{\text{Mg}^{2+}}$  increases, as observed. The constant value of  $m$  for the Ex state (Figure 6C) suggests that this RNA conformation gives about the same energetic advantage to  $\text{Mg}^{2+}$  relative to putrescine $^{2+}$  over its entire surface.

The ‘ensemble RNA’ used in these experiments is a collection of conformations intermediate between the native and extended states. At the  $\text{Mg}^{2+}$  and putrescine $^{2+}$  concentrations used to maintain  $\Gamma_{\text{Mg}^{2+}}$  values between 0.5 and 1.5 ions/RNA in Figure 6A and C, the average  $R_g$  is much less than that of the extended form (cf. Figure 3A, 1–10 mM putrescine $^{2+}$ ), which implies that the helical segments of the riboswitch are on average closer to each other than in the extended variant. (This is consistent with the known sta-

bilizing influence of  $Mg^{2+}$  on the kissing loop contacts of purine riboswitches (29,32.) The intermediate  $m$  value for the ensemble RNA is also consistent with reduced accessibility of RNA surfaces to putrescine $^{2+}$ , compared to the Ex state, but it is interesting to note that the partially compacted conformations of the ensemble show no hint of developing the regions with very high discrimination in favor of  $Mg^{2+}$  seen in the native structure. The very low  $m$  values seen for the N state at low  $\Gamma_{Mg^{2+}}$  probably correspond to  $Mg^{2+}$ -accessible volumes that only appear when the RNA tertiary structure is fully in place. If the A-riboswitch native structure could accommodate several  $Mg^{2+}$  ions in volumes that were highly inaccessible to putrescine $^{2+}$ , one might expect  $m$  to remain very small as  $\Gamma_{Mg^{2+}}$  increases. Instead, Figure 6C shows a constantly increasing value of  $m$  from the first value at  $\Gamma_{Mg^{2+}} = 0.5$  ions per RNA; we conclude that putrescine $^{2+}$  can access all but a small fraction of the RNA surface.

In summary, the model we present here is that the RNA folds from an extended form in which putrescine $^{2+}$  is equally disadvantaged in competing against  $Mg^{2+}$  throughout the RNA, to a tertiary structure with a more highly differentiated surface that strongly discriminates against putrescine $^{2+}$  in limited regions. As sketched in Figure 1B, putrescine $^{2+}$  interacts less strongly than  $Mg^{2+}$  with both Ex and N conformations of the riboswitch, but the difference is more pronounced with the native state. Although putrescine $^{2+}$  is nevertheless able to stabilize the A-riboswitch, presumably RNAs tertiary structures with more convoluted surfaces would interact even less strongly with putrescine $^{2+}$ ; likewise, partially unfolded RNAs with more structure than the highly extended state of the C60G RNA may be less favorable to putrescine $^{2+}$ . An extreme case is the very compact M box RNA, which takes up  $Mg^{2+}$  into several pockets that would be completely inaccessible to putrescine $^{2+}$  (41). This RNA readily folds when  $Mg^{2+}$  is present but is actually destabilized when putrescine $^{2+}$  is in excess over  $Mg^{2+}$  (14); putrescine $^{2+}$  therefore must interact more strongly with partially unfolded RNA than with the native fold. An implication of the present and previous (14) work is that the architectures of both folded and unfolded forms of an RNA determine how its stability responds to competing  $Mg^{2+}$  and putrescine $^{2+}$  ions.

Our model of  $Mg^{2+}$  versus putrescine $^{2+}$  competition is consistent with ideas put forward by others, who have argued from experiments and model calculations on the folding of large RNAs that the ability of a divalent ion to stabilize large RNA tertiary structure decreases in proportion to the ion's size (6). The competition experiments and free energy measurements presented here give a more quantitative picture of how the folding of an RNA structure influences the competition between the ions, and are unique in measuring free energies of ion – RNA interactions for specific RNA conformations (Figure 1), rather than just the net effect of ions on  $\Delta G^{\circ}_{\text{Fold}}$ . As such, the data provide benchmarks for computational studies that examine the relation between an RNA structure and the stabilizing ion atmosphere that surrounds it.

## SUPPLEMENTARY DATA

Supplementary Data are available at NAR Online.

## ACKNOWLEDGEMENTS

The authors thank Dr Xiaobing Zuo and Dr Yun-Xing Wang for assistance in obtaining and analyzing SAXS data.

## FUNDING

National Institutes of Health [RO1 GM58545 and T32 GM008403]; Francis D. Carlson Fellowship of the Department of Biophysics [to R.J.T.]. Funding for open access charge: School of Arts and Sciences, Johns Hopkins University.

*Conflict of interest statement.* None declared.

## REFERENCES

1. Draper, D.E. (2004) A guide to ions and RNA structure. *RNA*, **10**, 335–343.
2. Bai, Y., Greenfeld, M., Travers, K.J., Chu, V.B., Lipfert, J., Doniach, S. and Herschlag, D. (2007) Quantitative and comprehensive decomposition of the ion atmosphere around nucleic acids. *J. Am. Chem. Soc.*, **129**, 14981–14988.
3. Lambert, D., Leipply, D., Shiman, R. and Draper, D.E. (2009) The influence of monovalent cation size on the stability of RNA tertiary structures. *J. Mol. Biol.*, **390**, 791–804.
4. Stein, A. and Crothers, D.M. (1976) Conformational changes of transfer RNA. The role of magnesium(II). *Biochemistry*, **15**, 160–168.
5. Misra, V.K. and Draper, D.E. (2002) The linkage between magnesium binding and RNA folding. *J. Mol. Biol.*, **317**, 507–521.
6. Koculi, E., Hyeon, C., Thirumalai, D. and Woodson, S.A. (2007) Charge density of divalent metal cations determines RNA stability. *J. Am. Chem. Soc.*, **129**, 2676–2682.
7. Moghaddam, S., Caliskan, G., Chauhan, S., Hyeon, C., Briber, R.M., Thirumalai, D. and Woodson, S.A. (2009) Metal ion dependence of cooperative collapse transitions in RNA. *J. Mol. Biol.*, **393**, 753–764.
8. Woodson, S.A. (2010) Compact intermediates in RNA folding. *Annu. Rev. Biophys.*, **39**, 61–77.
9. Kuhn, A. and Kellenberger, E. (1985) Productive phage infection in *Escherichia coli* with reduced internal levels of the major cations. *J. Bacteriol.*, **163**, 906–912.
10. Capp, M.W., Cayley, D.S., Zhang, W., Guttman, H.J., Melcher, S.E., Saecker, R.M., Anderson, C.F. and Record, M.T. Jr (1996) Compensating effects of opposing changes in putrescine (2+) and K+ concentrations on lac repressor-lac operator binding: in vitro thermodynamic analysis and in vivo relevance. *J. Mol. Biol.*, **258**, 25–36.
11. Tabor, C.W. and Tabor, H. (1985) Polyamines in microorganisms. *Microbiol. Rev.*, **49**, 81–99.
12. Xie, Q.W., Tabor, C.W. and Tabor, H. (1993) Deletion mutations in the speED operon: spermidine is not essential for the growth of *Escherichia coli*. *Gene*, **126**, 115–117.
13. Chattopadhyay, M.K., Tabor, C.W. and Tabor, H. (2009) Polyamines are not required for aerobic growth of *Escherichia coli*: preparation of a strain with deletions in all of the genes for polyamine biosynthesis. *J. Bacteriol.*, **191**, 5549–5552.
14. Trachman, R.J. 3rd and Draper, D.E. (2013) Comparison of interactions of diamine and Mg(2+) with RNA tertiary structures: similar versus differential effects on the stabilities of diverse RNA folds. *Biochemistry*, **52**, 5911–5919.
15. Grilley, D., Soto, A.M. and Draper, D.E. (2006) Mg $^{2+}$ -RNA interaction free energies and their relationship to the folding of RNA tertiary structures. *Proc. Natl. Acad. Sci. U.S.A.*, **103**, 14003–14008.
16. Quigley, G.J., Teeter, M.M. and Rich, A. (1978) Structural analysis of spermine and magnesium ion binding to yeast phenylalanine transfer RNA. *Proc. Natl. Acad. Sci. U.S.A.*, **75**, 64–68.
17. Misra, V.K. and Draper, D.E. (2000) Mg(2+) binding to tRNA revisited: the nonlinear Poisson-Boltzmann model. *J. Mol. Biol.*, **299**, 813–825.

18. Soto, A.M., Misra, V. and Draper, D.E. (2007) Tertiary structure of an RNA pseudoknot is stabilized by 'diffuse' Mg(2+) ions. *Biochemistry*, **46**, 2973–2983.
19. Hayes, R.L., Noel, J.K., Whitford, P.C., Mohanty, U., Sanbonmatsu, K.Y. and Onuchic, J.N. (2014) Reduced model captures Mg(2+)-RNA interaction free energy of riboswitches. *Biophys. J.*, **106**, 1508–1519.
20. Grilley, D., Soto, A.M. and Draper, D.E. (2009) Direct quantitation of Mg2+-RNA interactions by use of a fluorescent dye. *Methods Enzymol.*, **455**, 71–94.
21. Leipply, D. and Draper, D.E. (2010) Dependence of RNA tertiary structural stability on Mg2+ concentration: interpretation of the Hill equation and coefficient. *Biochemistry*, **49**, 1843–1853.
22. Leipply, D. and Draper, D.E. (2011) Effects of Mg(2+) on the free energy landscape for folding a purine riboswitch RNA. *Biochemistry*, **50**, 2790–2799.
23. Semenyuk, A.V. and Svergun, D.I. (1991) GNOM—a program package for small-angle scattering data processing. *J. Appl. Crystallogr.*, **24**, 537–540.
24. Jacobson, D.R. and Saleh, O.A. (2016) Quantifying the ion atmosphere of unfolded, single-stranded nucleic acids using equilibrium dialysis and single-molecule methods. *Nucleic Acids Res.*, **44**, 3763–3771.
25. Leipply, D. and Draper, D.E. (2011) Evidence for a thermodynamically distinct Mg(2+) ion associated with formation of an RNA tertiary structure. *J. Am. Chem. Soc.*, **133**, 13397–13405.
26. Porter, E.B., Marcano-Velázquez, J.G. and Batey, R.T. (2014) The purine riboswitch as a model system for exploring RNA biology and chemistry. *Biochim. Biophys. Acta*, **1839**, 919–930.
27. Mandal, M. and Breaker, R.R. (2004) Adenine riboswitches and gene activation by disruption of a transcription terminator. *Nat. Struct. Mol. Biol.*, **11**, 29–35.
28. Serganov, A., Yuan, Y.R., Pikovskaya, O., Polonskaia, A., Malinina, L., Phan, A.T., Hobartner, C., Micura, R., Breaker, R.R. and Patel, D.J. (2004) Structural basis for discriminative regulation of gene expression by adenine- and guanine-sensing mRNAs. *Chem Biol*, **11**, 1729–1741.
29. Lemay, J.F., Penedo, J.C., Tremblay, R., Lilley, D.M. and Lafontaine, D.A. (2006) Folding of the adenine riboswitch. *Chem. Biol.*, **13**, 857–868.
30. Stoddard, C.D., Gilbert, S.D. and Batey, R.T. (2008) Ligand-dependent folding of the three-way junction in the purine riboswitch. *RNA*, **14**, 675–684.
31. Noeske, J., Schwalbe, H. and Wohnert, J. (2007) Metal-ion binding and metal-ion induced folding of the adenine-sensing riboswitch aptamer domain. *Nucleic Acids Res.*, **35**, 5262–5273.
32. Buck, J., Noeske, J., Wohnert, J. and Schwalbe, H. (2010) Dissecting the influence of Mg2+ on 3D architecture and ligand-binding of the guanine-sensing riboswitch aptamer domain. *Nucleic Acids Res.*, **38**, 4143–4153.
33. Draper, D.E. (2008) RNA folding: thermodynamic and molecular descriptions of the roles of ions. *Biophys. J.*, **95**, 5489–5495.
34. Lipfert, J., Doniach, S., Das, R. and Herschlag, D. (2014) Understanding nucleic acid-ion interactions. *Annu. Rev. Biochem.*, **83**, 813–841.
35. Heerschap, A., Walters, J.A.L.I. and Hilbers, C.W. (1985) Interactions of some naturally occurring cations with phenylalanine and initiator tRNA from yeast as reflected by their thermal stability. *Biophys. Chem.*, **22**, 205–217.
36. Bukhman, Y.V. and Draper, D.E. (1997) Affinities and selectivities of divalent cation binding sites within an RNA tertiary structure. *J. Mol. Biol.*, **273**, 1020–1031.
37. Koculi, E., Lee, N.K., Thirumalai, D. and Woodson, S.A. (2004) Folding of the Tetrahymena ribozyme by polyamines: importance of counterion valence and size. *J. Mol. Biol.*, **341**, 27–36.
38. Koculi, E., Thirumalai, D. and Woodson, S.A. (2006) Counterion charge density determines the position and plasticity of RNA folding transition states. *J. Mol. Biol.*, **359**, 446–454.
39. Misra, V.K. and Draper, D.E. (2001) A thermodynamic framework for Mg2+ binding to RNA. *Proc. Natl. Acad. Sci. U.S.A.*, **98**, 12456–12461.
40. Cate, J.H., Hanna, R.L. and Doudna, J.A. (1997) A magnesium ion core at the heart of a ribozyme domain. *Nat. Struct. Biol.*, **4**, 553–558.
41. Dann, C.E. 3rd, Wakeman, C.A., Sieling, C.L., Baker, S.C., Irnov, I. and Winkler, W.C. (2007) Structure and mechanism of a metal-sensing regulatory RNA. *Cell*, **130**, 878–892.
42. Zhang, J. and Ferre-D'Amare, A.R. (2014) Dramatic improvement of crystals of large RNAs by cation replacement and dehydration. *Structure*, **22**, 1363–1371.
43. Draper, D.E., Grilley, D. and Soto, A.M. (2005) Ions and RNA folding. *Annu. Rev. Biophys. Biomol. Struct.*, **34**, 221–243.
44. Noeske, J., Wasserman, M.R., Terry, D.S., Altman, R.B., Blanchard, S.C. and Cate, J.H. (2015) High-resolution structure of the Escherichia coli ribosome. *Nat. Struct. Mol. Biol.*, **22**, 336–341.
45. Correll, C.C., Freeborn, B., Moore, P.B. and Steitz, T.A. (1997) Metals, motifs, and recognition in the crystal structure of a 5S rRNA domain. *Cell*, **91**, 705–712.
46. Shi, H. and Moore, P.B. (2000) The crystal structure of yeast phenylalanine tRNA at 1.93 Å resolution: a classic structure revisited. *RNA*, **6**, 1091–1105.
47. Chin, K., Sharp, K.A., Honig, B. and Pyle, A.M. (1999) Calculating the electrostatic properties of RNA provides new insights into molecular interactions and function. *Nat. Struct. Biol.*, **6**, 1055–1061.
48. Kirmizialtin, S., Pabit, S.A., Meisburger, S.P., Pollack, L. and Elber, R. (2012) RNA and its ionic cloud: solution scattering experiments and atomically detailed simulations. *Biophys. J.*, **102**, 819–828.
49. Braunlin, W.H., Strick, T.J. and Record, M.T. Jr (1982) Equilibrium dialysis studies of polyamine binding to DNA. *Biopolymers*, **21**, 1301–1314.